International Journal on Engineering Technology and Infrastructure Development (InJET-InDev)
Volume 1, Issue No.1, Page 122-133
Received Date: 12/25/2023
Revised Date: 1/20/2024
Accepted Date: 2/10/2024
ISSN: 3021-999X (Print)

# Influence of Turbulence Models on Three-Dimensional Numerical Simulation of Downpull Phenomenon under Vertical Lift Gates

Khor Hao Zhe[1], Puay How Tion[2]

[1] *River Engineering and Urban Drainage Research Centre, Universiti Sains Malaysia, Nibong Tebal, Malaysia, khorhaozhe1018@student.usm.my*

[2] *River Engineering and Urban Drainage Research Centre, Universiti Sains Malaysia, Nibong Tebal, Malaysia, redac_puay@usm.my*

**Abstract**

One of the key concerns when operating a vertical lift gate is the underestimation of hydrodynamic downpull forces. Computational Fluid Dynamics (CFD) is an effective method in simulating downpull phenomenon under vertical lift gates. The purpose of this study is to investigate the effect of turbulence models on the numerical simulation of downpull phenomenon under vertical lift gates using Flow-3D®, a commercial CFD software. The downpull phenomenon is simulated using three different turbulence models, which are standard k-$\varepsilon$ model, k-$\omega$ two-equation model and LES model. The simulations are done for nine different gate opening sizes using the three aforementioned turbulence models. The setup of numerical model is identical to experiment setup used by Naudascher in 1964. The results showed that standard k-$\varepsilon$ model showed the least deviation from experimental results with an average percentage error of 11.365%.

*Keywords*: Vertical lift gate, Numerical Model, Downpull Force, Turbulence Model

## 1. Introduction

### *1.1. Vertical Lift Gates and Downpull Forces*

Vertical lift gates are often used as emergency gate to control the inflow into pipe at dam intake structures due to its simple operation method and requirement of little maintenance (Erbisti, 2004). The emergency gate is designed so that it is watertight and can completely isolate the flow in the intake tower from entering the intake pipe. Emergency gates are usually designed so that it is capable of closing under its self-weight. To lift the gate, the self-weight of the gate, friction from the gate wheel, resistance force due to friction as well as hydrodynamic forces are considered (Lewin, 2021). During the lifting process, the flow under the gate can generate a substantial amount of hydrodynamic down pull force. This down pull force is the result of high velocity flow at the bottom of the gate which creates a zone of low pressure. Hence, the pressure difference between top and bottom part of the gate causes a strong downwards force to be generated (Naudascher et al., 1964). The down pull force causes an additional resisting force to the gate hoisting system. Miscalculation of the hydrodynamic down pull force can seriously damage gate hoists. Therefore, it is critical to accurately predict the additional down pull forces to ensure safe operation of emergency gates.

### *1.2. Computational Fluid Dynamics (CFD)*

Computational Fluid Dynamics (CFD) is a modern mathematical method used in modelling fluid flow cases and solve the problem numerically with computers. One of the main parts of CFD involves substituting the governing equation for fluid flow, which is cast in partial differential form with numbers. The result obtained through the manipulation of equations will be a collection of numbers. Numbers are very crucial in any engineering analysis, as in most cases, the objective is to acquire the quantitative description of the problem (Anderson et al., 2009).

There are three main components in CFD, which are algorithm development, grid generation and turbulence modeling. Highly accurate mathematical models have been developed over the years for algorithm development and grid generation. However, significantly less precision has been achieved for turbulence modeling due to the intricacy of the physical behavior of turbulent flows (Wilcox, 2006). Hence, choosing the appropriate turbulence model according to the specific characteristics of the simulated phenomenon is a critical decision that can significantly impact the accuracy of the results. Some common factors that influence the choice of turbulence model being used include boundary layer characteristics, computational cost, solver stability and convergence.

### *1.2. Flow-3D*

.

Flow-3D® is a commercial CFD software which is well known for its advancement in three-dimensional volume of fluid (VOF) algorithm and is frequently used in free surface flow analysis. It is also known for its ability to provide detailed analysis on even small-scaled simulations (Hu et al., 2018). In this study, Flow-3D® is used to simulate the downpull phenomenon under high head gates using three different turbulence models, which are standard k-$\varepsilon$ model, k-$\omega$ two-equation model and Large Eddy Simulation (LES) model.

The incompressible three-dimensional continuity and Navier-stokes equation are used to solve motion of fluids in Flow-3D®. The equations are denoted in Einstein's summation convention form as shown below:

$$\frac{\partial u_i}{\partial x_i} = 0 \tag{1}$$

$$\frac{\partial u_i}{\partial t} + u_j \frac{\partial u_i}{\partial x_j} = -\frac{1}{\rho} \frac{\partial P}{\partial x_i} + g_i + \frac{1}{\rho} \frac{\partial T_{ij}}{\partial x_j} \tag{2}$$

$$T_{ij} = 2\mu S_{ij}, \tag{3}$$

$$S_{ij} = \frac{1}{2}\left(\frac{\partial u_i}{\partial x_j} + \frac{\partial u_j}{\partial x_i}\right) \tag{4}$$

where $u_i$ is the velocity, $g_i$ is the gravitational acceleration, $\rho$ is the fluid density, $P$ is the pressure and $T_{ij}$ is the stress tensor.

### *1.3. Turbulence Models*

#### *1.3.1. Reynolds-Averaged Navier-Stokes Model*

The standard k-$\varepsilon$ model and k-$\omega$ two-equation model are Reynolds-Averaged Navier-Stokes (RANS) turbulence models. RANS is an approach used to simulate turbulent flows by decomposing flow variables into time-averaged and fluctuating components. By time-averaging equations (1) and (2), Reynolds averaged equations of motion can be yielded as shown below:

$$\frac{\partial U_i}{\partial x_i} = 0 \tag{5}$$

$$\frac{\partial U_i}{\partial t} + U_j \frac{\partial U_i}{\partial x_j} = -\frac{1}{\rho} \frac{\partial P}{\partial x_i} + g_i + \frac{1}{\rho} \frac{\partial}{\partial x_j}(2\mu S_{ji} + \rho\tau_{ij}) \tag{6}$$

$$\tau_{ij} = -\overline{u_j' u_i'} \tag{7}$$

where most of the terms are identical to each other with the difference of replacing instantaneous variables in equations (1) and (2) with mean values for the variables. Another difference is the addition of the correlation $\tau_{ij}$, which is the specific Reynolds stress-tensor. According to Boussinesq hypothesis, at all points in a turbulent flow, the primary axes of the Reynolds stress-tensor correspond with those of the mean rate of strain tensor (Wilcox, 2006). Hence, the Reynolds stress-tensor can be expressed as:

$$\tau_{ij} = 2\mu_T S_{ij} - \frac{2}{3}k\delta_{ij} \tag{8}$$

where $\mu_T$ is the eddy viscosity, $S_{ij}$ is the mean rate of strain tensor, $k$ is the kinetic energy of turbulent fluctuations per unit mass and $\delta_{ij}$ is the Kronecker delta.

The standard k-$\varepsilon$ model is a two-equation turbulence model, where two transport equations are solved for two different quantities, namely the turbulent kinetic energy, $k$ and specific dissipation rate, $\omega$. These two quantities can then be related to determine the value for eddy viscosity, $\mu_T$. The transport equations for these quantities and relation between them and eddy viscosity are expressed as follow:

$$\frac{\partial k}{\partial t} + U_j\frac{\partial k}{\partial x_j} = \frac{1}{\rho}\tau_{ij}\frac{\partial U_i}{\partial x_j} - \varepsilon + \frac{1}{\rho}\frac{\partial}{\partial x_j}\left[\left(\mu + \frac{\mu_T}{\sigma_k}\right)\frac{\partial k}{dx_j}\right] \tag{9}$$

$$\frac{\partial \varepsilon}{\partial t} + U_j\frac{\partial \varepsilon}{\partial x_j} = C_{\varepsilon 1}\frac{\varepsilon}{\rho k}\tau_{ij}\frac{\partial U_i}{\partial x_j} - C_{\varepsilon 2}\frac{\varepsilon^2}{k} + \frac{1}{\rho}\frac{\partial}{\partial x_j}\left[\left(\mu + \frac{\mu_T}{\sigma_\varepsilon}\right)\frac{\partial \varepsilon}{dx_j}\right] \tag{10}$$

$$\mu_T = \rho C_\mu \frac{k^2}{\varepsilon}$$

where default values for closure coefficients are given by Flow-3D as $\sigma_k = 1.0$, $\sigma_\varepsilon = 1.39$, $C_{\varepsilon 1}$=1.44, $C_{\varepsilon 2}$=1.92 and $C_\mu = 0.085$.

The k-$\omega$ two-equation model works in a very similar manner, with the difference of solving transport equation for specific dissipation rate, $\omega$ instead of dissipation rate, $\varepsilon$. Eddy viscosity is then determined through another relation between specific dissipation rate and turbulent kinetic energy. The transport equations for $k$ and $\omega$, as well as the relation between them with eddy viscosity are expressed as follow:

$$\frac{\partial k}{\partial t} + U_j\frac{\partial k}{\partial x_j} = \frac{1}{\rho}\tau_{ij}\frac{\partial U_i}{\partial x_j} - \beta^* k\omega + \frac{1}{\rho}\frac{\partial}{\partial x_j}\left[\left(\mu + \sigma^*\rho\frac{k}{\omega}\right)\frac{\partial k}{dx_j}\right] \tag{11}$$

$$\frac{\partial \omega}{\partial t} + U_j\frac{\partial \omega}{\partial x_j} = \frac{\alpha}{\rho}\tau_{ij}\frac{\partial U_i}{\partial x_j} - \beta\omega^2 + \frac{1}{\rho}\frac{\partial}{\partial x_j}\left[\left(\mu + \sigma\rho\frac{k}{\omega}\right)\frac{\partial \omega}{dx_j}\right] \tag{12}$$

$$\mu_T = \rho\frac{k}{\omega} \tag{13}$$

$$\beta^* = \beta_0^* f_{\beta^*} \tag{14}$$

$$f_{\beta^*} = \begin{cases} 1, & \chi_k \le 0 \\ \dfrac{1 + 680\chi_k^2}{1 + 400\chi_k^2}, & \chi_k > 0 \end{cases} \tag{15}$$

$$\chi_k \equiv \frac{1}{\omega^3}\left(\frac{\partial k_T}{\partial xi}\frac{\partial \omega_T}{\partial x_i}\right) \tag{16}$$

$$\beta = \beta_0 f_\beta \tag{17}$$

$$f_{\beta^*} = \frac{1 + 70\chi_\omega}{1 + 80\chi_\omega} \tag{18}$$

$$\chi_\omega \equiv \left|\frac{\Omega_{ij}\Omega_{jk}S_{ki}}{(\beta_0^*\omega)^3}\right| \tag{19}$$

$$\Omega_{ij} = \frac{1}{2}\left(\frac{\partial U_i}{\partial x_j} - \frac{\partial U_j}{\partial x_i}\right) \tag{20}$$

where default values for closure coefficients are given by Flow-3D as $\alpha = 0.52$, $\beta_0^* = 0.09$, $\beta_0 = 0.072$, $\sigma^* = 0.5$ and $\sigma = 0.5$.

### *1.3.2. Large Eddy Simulation (LES) Model*

Large Eddy Simulation (LES) is a computational approach used in CFD in which large eddies are explicitly resolved and smaller-scaled eddies are modeled. A filtering process is done to decompose flow variables to large-scale (resolved) components and small-scale (unresolved) components (Wilcox, 2006). This is usually done

through spatial filter that removes high-frequency fluctuations. A finer mesh size is usually recommended when using LES models to capture the large-scale components better.

For turbulences that are too small to compute, an eddy viscosity is used as representation which proportionate to a length scale times a measure of velocity fluctuations of that scale. For the length scale, $L$, a geometric mean of the grid cell dimensions is used. The eddy viscosity, $\mu_T$can then be computed as follow:

$$L = \left(\delta_x \delta_y \delta_z\right)^{\frac{1}{3}} \tag{21}$$

$$\mu_T = \rho(C_s L)^2 \cdot \sqrt{S_{ij} S_{ij}} \tag{22}$$

where $L$ is the length scale and $C_s$ is the Smagorinsky coefficient with a typical value in the range of 0.1 to 0.2.

## 2. Methodology

Flow-3D® is used to simulate flow under vertical lift gates. Incompressible flow (for water) is selected as the type of flow and the simulation time is set to 15 seconds for each run and an additional condition of stopping the simulation once steady state is achieved is also set. A total of 27 simulations were carried out according to different gate opening sizes and turbulence models used. Three different cases varied by turbulence models were considered in this study. Simulations under 9 different gate opening sizes for each case were considered, which ranges from 10% to 90% with 10% increment interval. The numerical results obtained are then compared to experimental results by Naudascher in 1964 for validation purposes (Naudascher et al., 1964).

### *2.1. Gate Geometry*

The vertical lift gate model used was prepared using AUTOCAD 3D software and exported as stereolithography (STL) file to be used in Flow-3D as an obstacle. The geometry and dimensions of the gate is shown in Figure 1.

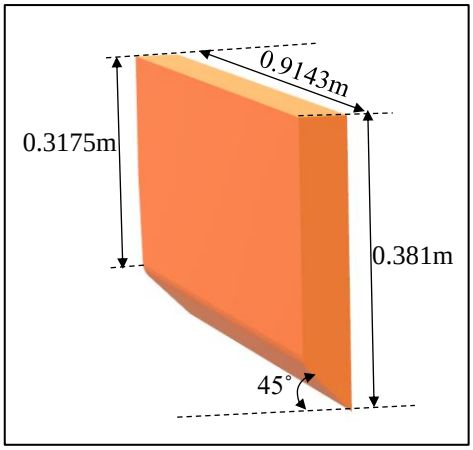


Figure 1. Geometry of gate model

### *2.2. Simulation domain and meshing*

The simulation domain used is shown in Figure 2. Uniform cartesian mesh was used for all mesh blocks. Coarser grid sizes of 0.01m were used for mesh block 1 and mesh block 2. Mesh block 3 uses a finer cell size of 0.005m to resolve the finer features at the bottom part of the gate geometry. The width for each mesh block was fixed at 0.9143m. Each mesh block has different lengths, mesh block 1 is 0.27m long, mesh block 2 is 0.64m long and mesh block 3 is just 0.0635m long. Different heights were used for each mesh block according to gate opening size. The heights used for each mesh block differentiated by gate opening size is summarized in Table 1.

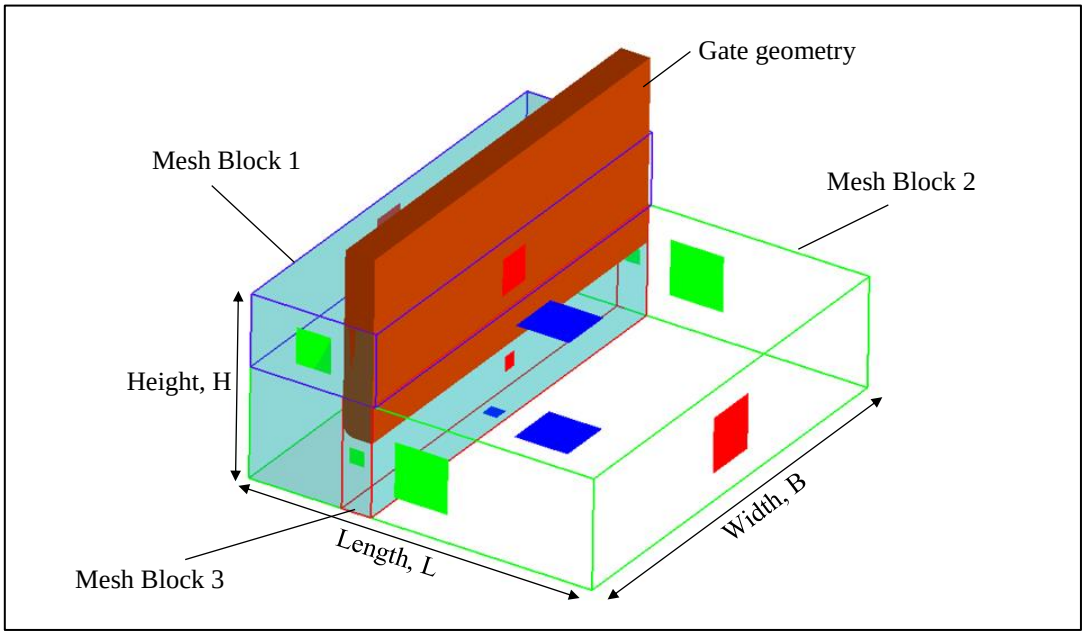


Figure 2. Simulation domain

Table 1. Heights for mesh blocks differentiated by gate opening size

| Gate Opening Size (%) | Height, H (m) | | |
|---|---|---|---|
| | Mesh block 1 | Mesh block 2 | Mesh block 3 |
| 10 | 0.13 | 0.13 | 0.251 |
| 20 | 0.16 | 0.16 | 0.221 |

| | | | |
|---|---|---|---|
| 30 | 0.19 | 0.19 | 0.191 |
| 40 | 0.23 | 0.23 | 0.151 |
| 50 | 0.27 | 0.27 | 0.111 |
| 60 | 0.31 | 0.31 | 0.071 |
| 70 | 0.35 | 0.35 | 0.031 |
| 80 | 0.381 | 0.381 | 0 |
| 90 | 0.381 | 0.381 | 0 |

### *2.3. Boundary Condition*

The upstream boundary was defined as an inflow boundary where the inflow velocity is set based on the gate opening size. The inflow velocity is adjusted to control the downstream efflux velocity to be within a range of 22.86ms$^{-1}$ to 25.91ms$^{-1}$. The downstream boundary was set to be an outflow boundary to allow fluid to smoothly propagate out of the domain without reflection. Wall boundaries are used for the sides of the computational domain to prevent fluid from moving through the boundaries. The wall is set as non-slip surface.

### *2.4. Downpull Coefficient*

Downpull force is primarily caused by the pressure difference between a gate's top and bottom surfaces. To simplify the process of determining downpull forces, a dimensionless downpull coefficient, K, was derived from previous research studies. To forecast the pressure forces acting on the gate, these dimensionless coefficients are derived based on the ratio of the corresponding mean piezometric head to a reference velocity head (Naudascher et al., 1964). The importance of the obtained "K-terms" is that they are independent of the absolute flow velocity magnitude. They can be employed in any flow condition as long as the boundary geometry is identical and the Reynolds number is sufficiently high, which is generally the case for high-head gates.

$$K_B = \frac{h_i - h_j}{\frac{v_j^2}{2g}} \tag{23}$$

where $h_i$ is the piezometric head at the bottom surface of the gate, $h_j$ and $v_j$ are the piezometric head and flow velocity at a contracted jet located downstream respectively. The location of the measured contracted jet is fixed to be at a distance of 1.25 times the gate opening size downstream of the gate. The values for $h_i$ are taken along 13 horizontal cross sections under the gate geometry, with each horizontal cross section having 184 sets of data. The values for $h_j$ and $v_j$ on the other hand are also taken along one horizontal cross section with each section having 92 sets of data. Bottom downpull coefficient obtained from simulation results are then compared to experimental results by Naudascher for validation purposes. Deviation from experimental results is calculated as percentage error with the following formula:

$$\text{Percentage error} = \left|\frac{\text{Simulation results} - \text{Experimental results}}{\text{Experimental results}}\right| \times 100\% \tag{23}$$

Mean percentage error, minimum percentage error and maximum percentage error are also determined for each case. Box-and-whisker plots were also drawn to provide visual summary for key statistics to highlight the central tendency, spread and skewness for each set of data.

## 3. Results and Discussion

Figure 3, Figure 4 and Figure 5 shows visualization of the numerical results for standard k-$\varepsilon$ model, k-$\omega$ two-equation model and LES model at 10%, 50% and 90% gate opening sizes. The derivation from experimental results is determined as shown in Table 2.

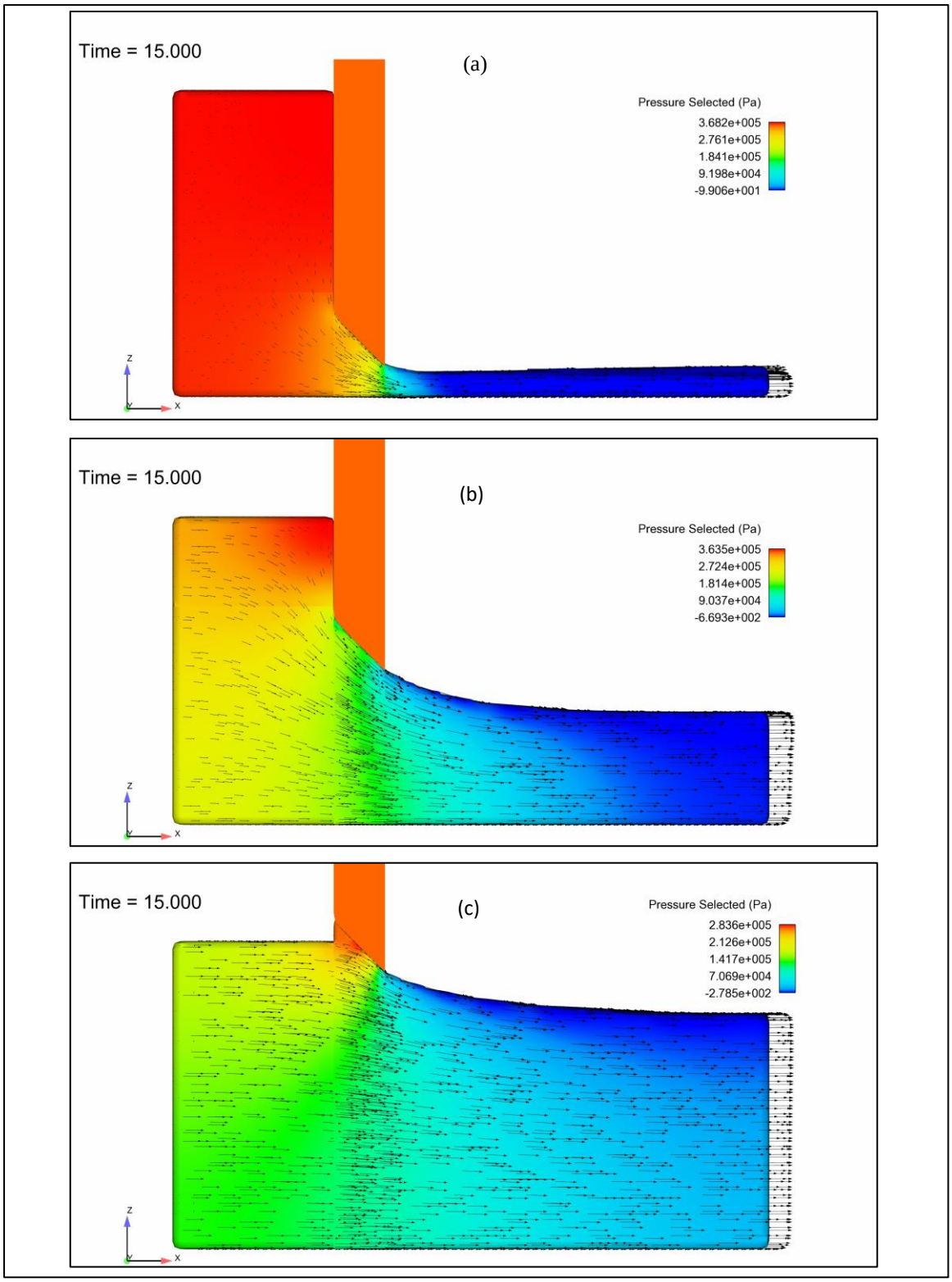


Figure 3. Visualization of numerical results for simulation with standard k-$\varepsilon$ model at (a) 10%, (b) 50% and (c) 90% gate opening size.

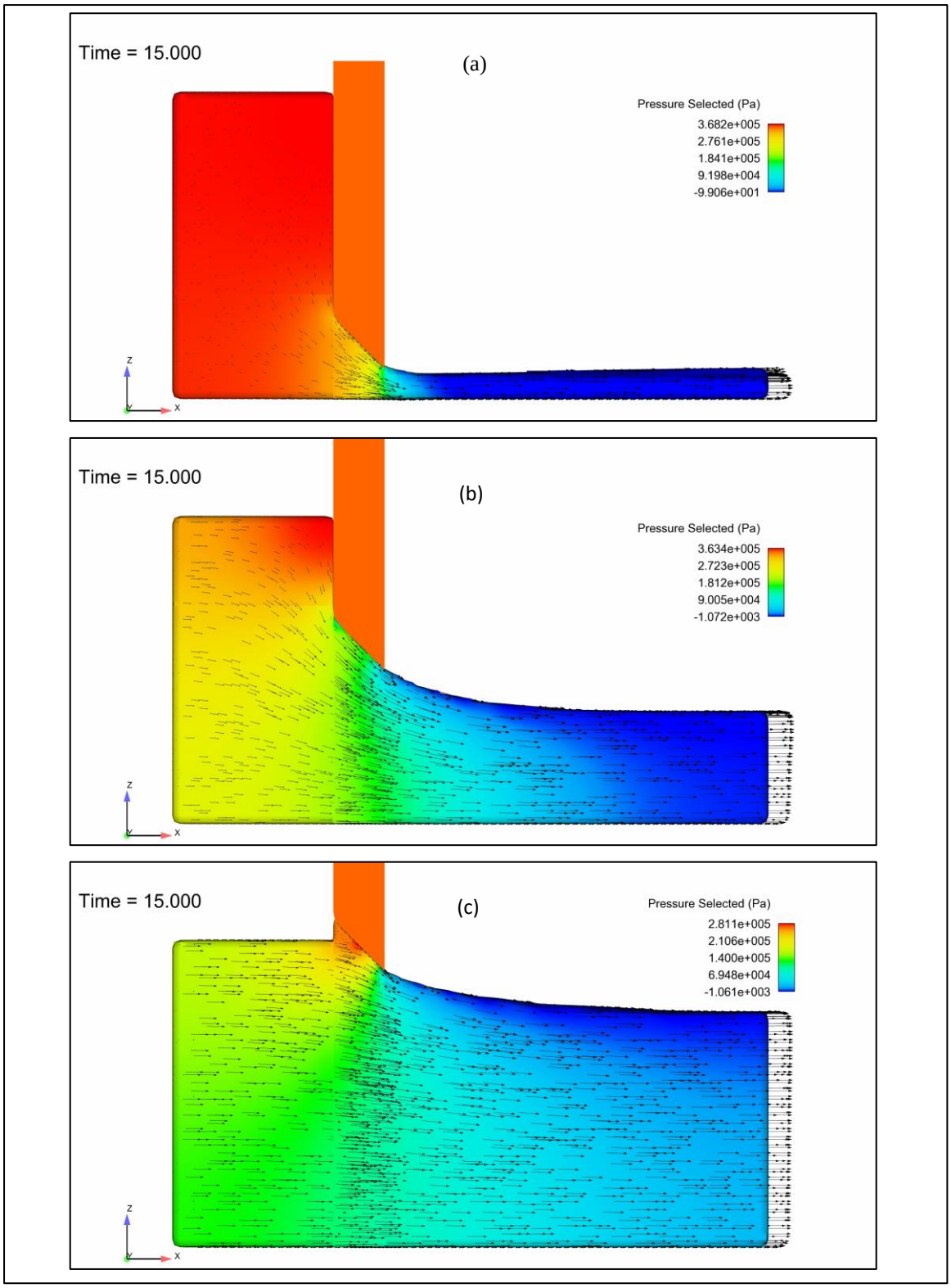


Figure 4. Visualization of numerical results for simulation with k-$\omega$ two-equation model at (a) 10%, (b) 50% and (c) 90% gate opening size.

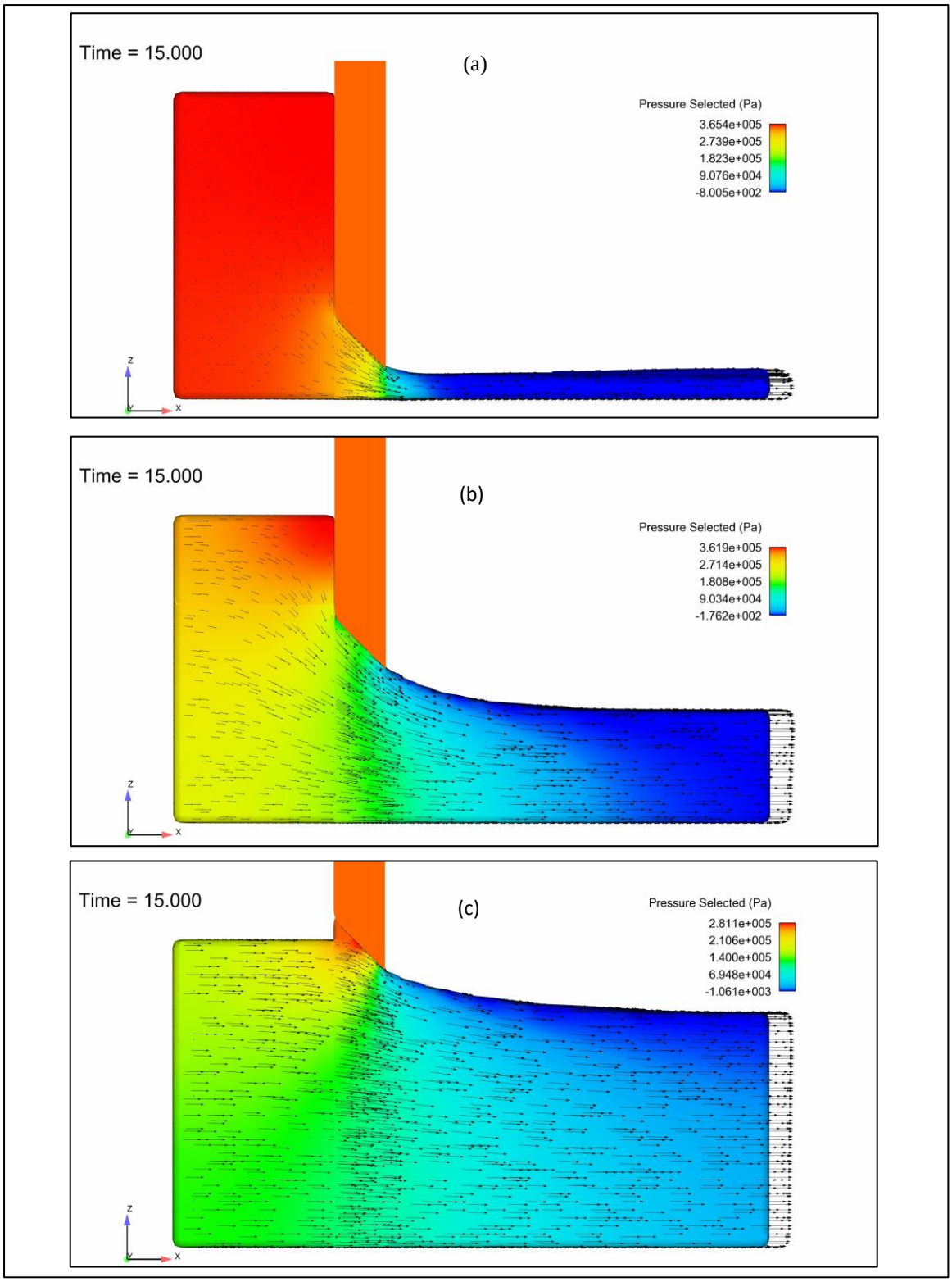


Figure 5. Visualization of numerical results for simulation with LES model at (a) 10%, (b) 50% and (c) 90% gate opening size.

Table 2. Deviation of Simulation Results from Experimental Results

| Gate Opening Size (%) | Percentage Error (%) | | | | | | | | |
|---|---|---|---|---|---|---|---|---|---|
| | standard k-$\varepsilon$ model | | | k-$\omega$ two-equation model | | | LES model | | |
| | Mean | Minimum | Maximum | Mean | Minimum | Maximum | Mean | Minimum | Maximum |
| 10 | 5.916 | 5.150 | 12.423 | 6.197 | 5.379 | 11.606 | 6.254 | 5.720 | 9.967 |
| 20 | 1.661 | 0.147 | 2.345 | 2.080 | 0.251 | 2.745 | 1.665 | 0.147 | 2.345 |
| 30 | 9.990 | 2.524 | 10.628 | 12.319 | 9.080 | 12.788 | 19.130 | 14.743 | 19.555 |
| 40 | 9.101 | 4.521 | 9.628 | 23.454 | 15.271 | 24.185 | 25.933 | 18.444 | 26.646 |
| 50 | 21.555 | 15.876 | 22.148 | 21.602 | 16.060 | 22.206 | 24.283 | 18.842 | 24.568 |
| 60 | 10.074 | 2.963 | 10.516 | 9.493 | 0.366 | 9.977 | 12.908 | 2.247 | 13.209 |
| 70 | 3.062 | 2.054 | 7.260 | 3.764 | 1.205 | 5.757 | 3.511 | 1.125 | 4.918 |
| 80 | 7.438 | 6.076 | 18.937 | 18.055 | 17.517 | 32.635 | 35.32 | 22.154 | 45.793 |
| 90 | 33.490 | 32.992 | 45.360 | 33.553 | 32.992 | 45.360 | 38.322 | 37.425 | 58.130 |
| **Average** | **11.365** | **8.034** | **15.472** | **14.502** | **10.902** | **18.584** | **18.591** | **13.427** | **22.792** |

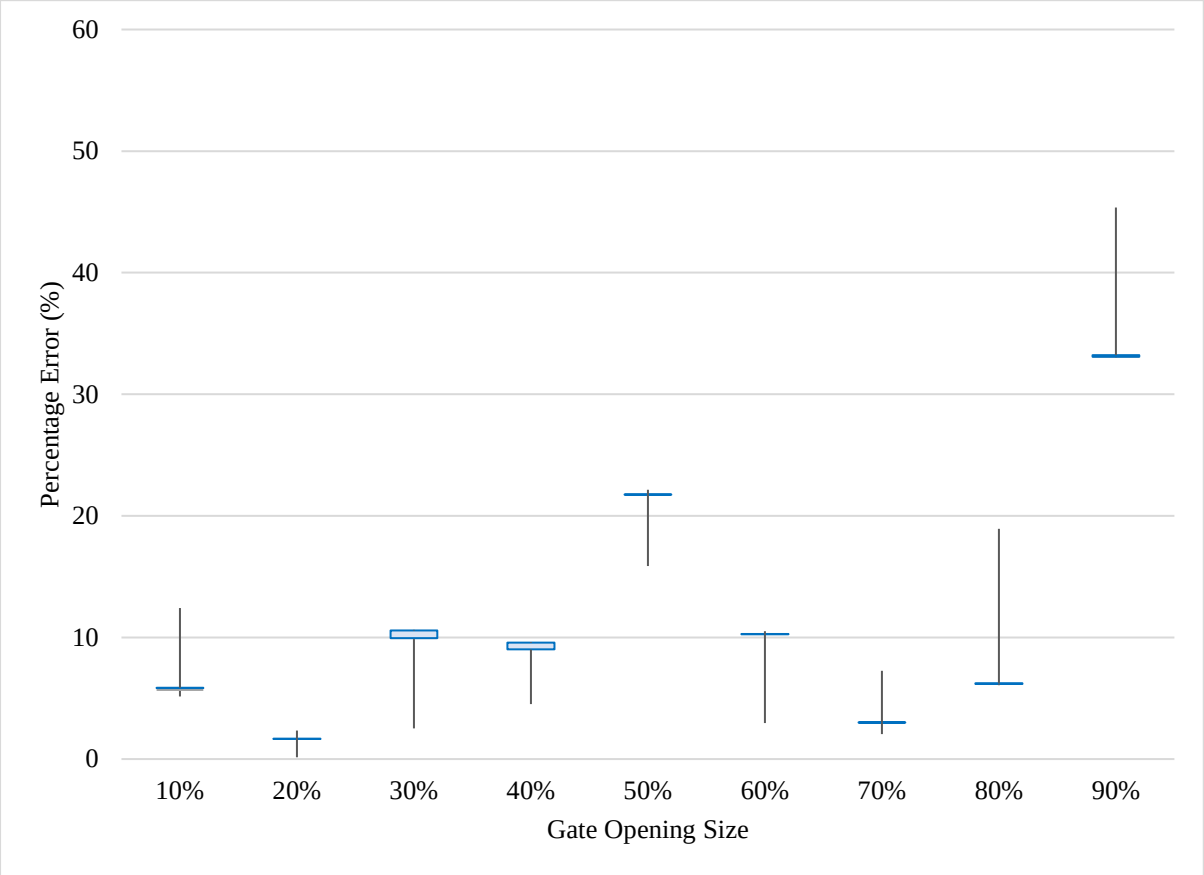


Figure 6. Distribution of Percentage Error Across Different Gate Opening Sizes (Standard k-$\varepsilon$ Model)

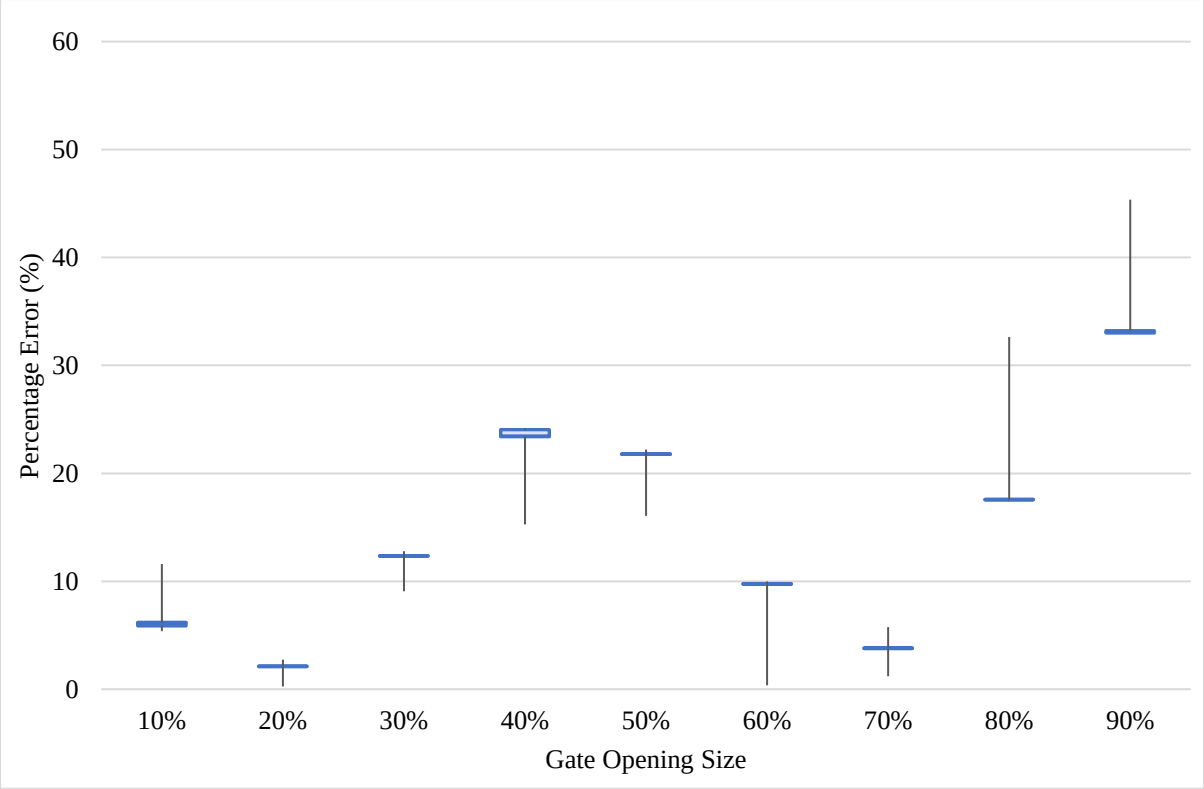


Figure 7. Distribution of Percentage Error Across Different Gate Opening Sizes (k-$\omega$ Two-Equation Model)

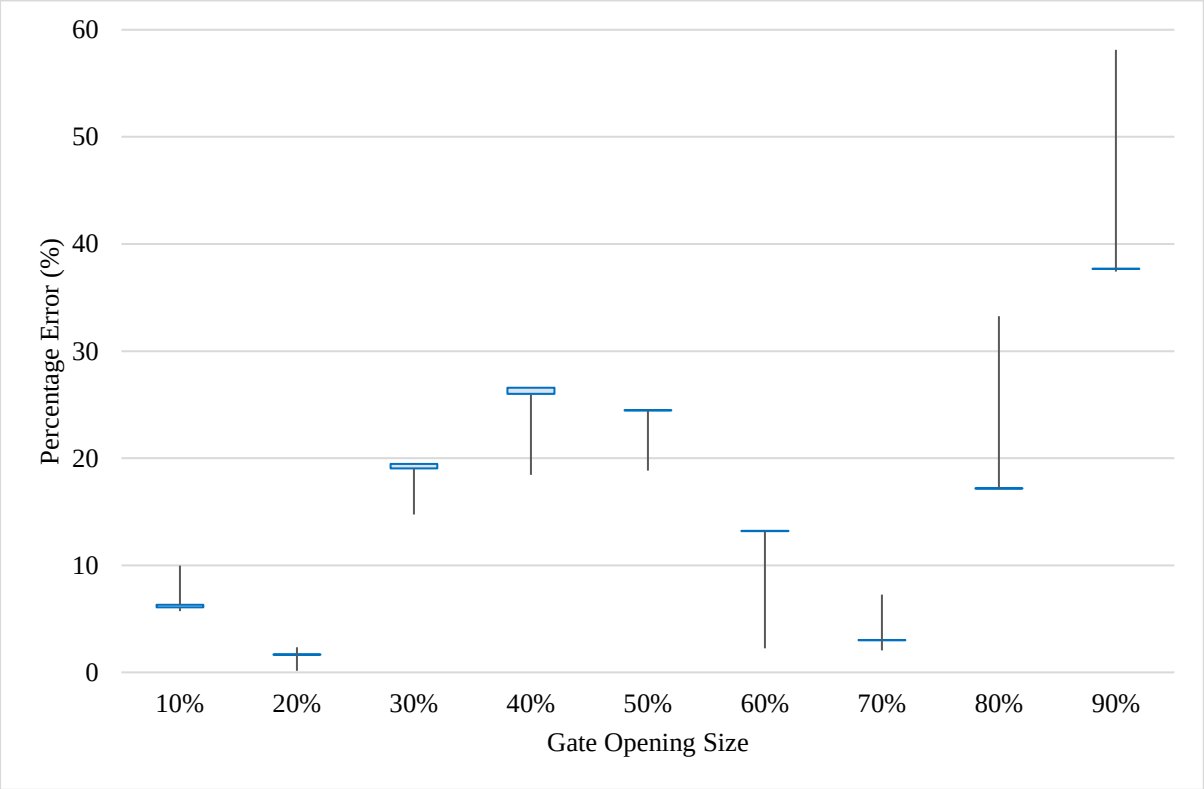


Figure 8. Distribution of Percentage Error Across Different Gate Opening Sizes (k-$\omega$ Two-Equation Model)

From the results shown in Table 2, standard k-$\varepsilon$ model recorded the lowest average in terms of mean percentage error at 11.365%, followed by k-$\omega$ two-equation model with 14.502% average mean percentage error and LES model has the highest mean percentage error (18.591%).

The length of each "boxes" in the box-and-whisker plots in Figure 6, Figure 7 and Figure 8 indicates the spread of the central 50% of data. It can be observed that the "boxes" for all simulations are relatively short, which indicates a small spread with less dispersion or variability in the central portion of each set of data. The only cases where there is a relatively larger spread of central 50% data is the simulation results for 40% gate opening sizes, as shown by the greater length of the "box".

The "whiskers" in the plot shows the values outside the interquartile range, as well as providing a visualization on the skewness for each plot. From the box-and-whisker plots in Figure 6, Figure 7 and Figure 8, it can first be observed that there is an inconsistent trend in terms of skewness for different gate opening sizes. However, if compared between results between different turbulence models, the trend for skewness is consistent across all models. Simulation results for 10%, 70%, 80% and 90% gate opening sizes showed negative skewness while results for the other gate opening sizes showed positive skewness for percentage error.

## 4. Conclusion

Standard k-$\varepsilon$ model shows the highest accuracy when it comes to determining bottom downpull coefficient under vertical lift gates in comparison to k-$\omega$ two-equation model or LES model. However, a mean percentage error of 11.365% is still far from ideal. There may be other contributing factors towards this accuracy such as mesh resolution or method of obstacle representation. Especially in terms of mesh resolution, if applicable, LES model may achieve much greater accuracy with finer mesh sizes. For future works, newer and enhanced turbulence models such as the SST k-omega model or even hybrid turbulence models such as hybrid RANS-LES models can also be used for further testing.

## References

Anderson, J. D., Degrez, G., Dick, E., & Grundmann, R. 1992. *Computational Fluid Dynamics: An Introduction,* Heidelberg: Springer Berlin.

Erbisti P.C.F, 2004. *Design of Hydraulic Gates,*Lisse: Swets&Zeitlinger Publishers.

Hu, X., Ran, D., & Wang, W. 2018. 'Three-dimensional Numerical Simulation of Flow in Trapezoidal Cutthroat Flumes Based on FLOW-3D', *Frontiers of Agricultural Science and Engineering*, vol. 5, no. 2, pp. 168-176.

Kim, S.W., 1988. 'A Near-Wall Turbulence Model and Its Application to Fully Developed Turbulent Channel and Pipe Flows', *NASA Technical Memorandum 101399,* Washington DC: National Aeronautics and Space Administration

Lewin,J. 2021. *Hydraulic Gates and Valves in Free Surface Flow and Submerged Outlets*, 2nd Edition, Victoria:Thomas Telford Limited.

Naudascher, E., ASCE M., Kobus, H. E., & Rao, R. P. R. 1964. 'Hydrodynamic Analysis for High-Head Leaf Gates', *Journal of the Hydraulics Division*, vol. 90, pp. 155-192.

Wilcox, D.C., 2006. *Turbulence Modeling for Cfd,* 3rd Edition, California: DCW Industries, Inc.